Key Points:
- A high-resolution study was conducted of bulk properties in a peat sequence from the Xinjiang Altai Mountains of northwest China
- Reconstructions of Holocene peat C and N accumulations in the Altai Mountains of northwest China were done
- Regional comparisons imply that plant communities and productivities are major controls on peat C and N accumulation in northwest China

Correspondence to:
Y. Zhang, S. Zhang, and P. A. Meyers,
zhangyan7299@126.com;
zhangshaoqing@neigae.ac.cn;
pameyers@umich.edu

Peat Properties and Holocene Carbon and Nitrogen Accumulation Rates in a Peatland in the Xinjiang Altai Mountains, Northwestern China

Yan Zhang[1,2], Ping Yang[1,2], Chuanyu Gao[3], Chuan Tong[1,2], Xinyan Zhang[4], Xingtu Liu[3], Shaoqing Zhang[3], and Philip A. Meyers[5]

[1]Key Laboratory of Humid Subtropical Eco-Geographical Process, Ministry of Education, Institute of Geographical Sciences, Fujian Normal University, Fuzhou, China, [2]Research Centre of Wetlands in Subtropical Region, Institute of Geographical Sciences, Fujian Normal University, Fuzhou, China, [3]Key Laboratory of Wetland Ecology and Environment, Northeast Institute of Geography and Agroecology, Chinese Academy of Sciences, Changchun, China, [4]School of Chemistry and Environmental Engineering, Changchun University of Science and Technology, Changchun, China, [5]Department of Earth and Environmental Sciences, The University of Michigan, Ann Arbor, MI, USA

Abstract A high-resolution study of bulk properties in a peat sequence from the Xinjiang Altai Mountains of northwestern China has allowed reconstruction of local variations in peat properties and peat C and N accumulation rates (CAR and NAR) during the Holocene. Analyses of peat bulk density, loss on ignition, and concentrations of total organic carbon (TOC) and total nitrogen (TN) and their elemental ratios and stable isotopic values suggest that changes in peat-forming vegetation types during different parts of this epoch are the major factors responsible for the variations of peat properties in this sequence. The long-term peat CAR has been 25.4 ± 7.7 (SD) g C/m^2/yr, with lower values during the early Holocene and higher accumulations during the late Holocene, which is opposite to the Holocene variations in CAR in other northern peatlands. In contrast, the long-term peat NAR is 1.5 ± 0.5 (SD) g N/m^2/yr and is higher during the early and middle Holocene and lower during the late Holocene as in other northern peatlands. However, unlike other northern peatlands, long-term peat NAR does not vary with the CAR, which is influenced by the peat density and accumulation rate. Variations in long-term peat C and N accumulations in the Altai Mountains can be attributed to changes in primary productivity, in the dominant plant types and in peat decomposition caused by changes in both regional Holocene climate and local conditions.

Plain Language Summary Variations in Holocene carbon and nitrogen accumulations in a peat sequence in the Altai Mountains of northwestern China can be attributed to changes in plant productivity, in the dominant plant types and in peat decomposition caused by changes in both regional climate and site-specific environmental conditions.

1. Introduction

Northern peatlands hold about a third of the global reduced carbon (C) pool (Gorham, 1991) and hence have essential roles in the global carbon cycle and the climate system (e.g., Gorham, 1991; Loisel et al., 2014; Yu, 2012; Yu et al., 2010). Climate is the dominant control on peat development and is the key driver of long-term C accumulation in peatlands, with both temperature and precipitation playing important roles in primary production and peat decomposition (e.g., Gorham, 1991; Lacourse & Davies, 2015; Panait et al., 2017; Yu et al., 2010). In general, periods of warmer and wetter climate are the principal controls on increased CAR by stimulating greater primary production that can offset peat decomposition (Loisel et al., 2014). Moreover, local factors such as topography, plant species composition, hydrological conditions, nutrient availability, and human disturbance are also important to peatland development (Lacourse & Davies, 2015; Larsson et al., 2017; Panait et al., 2017). Therefore, continued study of peatlands is warranted for assessing the interactions between climate changes and local factors for better understanding of peat development and its long-term C accumulation, especially in those regions that are lacking comprehensive peat studies (Lacourse & Davies, 2015).

Some large-scale syntheses have focused on peatlands in northern and subarctic regions, exploring the responses of peatland development histories and their C dynamics to global climate changes (e.g., Jones & Yu, 2010; Page et al., 2006; Smith et al., 2004; Tarnocai et al., 2009; Turunen et al., 2002; Xing et al., 2015; Zhao et al., 2014). The Asian monsoon and the westerlies play important inter-active roles in affecting changes in the climate of Asia, which might result in differences of peatland initiation and long-term peat C accumulation and their dominant controls under different regional climatic scenarios (Zhao et al., 2014). Studies mostly have synthesized peatland initiation and peat C accumulation histories in the different regions of China that are affected by monsoon rains. For example, the variations of net primary productivity (NPP) closely linked with summer insolation and monsoon intensities are the main factor in determining long-term peat C accumulation in Asian monsoon regions (e.g., Xing et al., 2015; Yu et al., 2010; Zhao et al., 2014). The arid and semi-arid areas in northwest China that are in the center of the Eurasian continent on the northern margin of the Tibetan Plateau are particularly sensitive to climate changes, and the climate of this region is influenced by more interactional climate systems than most other regions in Asia (e.g., Luo et al., 2009; Madsen et al., 2003; Zhang et al., 2016, 2018). However, a significant information gap about peat development and peat C accumulation remains in northwestern China, which is an area that is also influenced by complicated climate systems. Hence, much remains to be learned on a large regional scale to better understand the responses of northern peatland development and peat C accumulation to global climate changes under different ecologic-climatic scenarios.

In addition to C, large amounts of nitrogen (N) are stored in the northern peatlands (Limpens et al., 2006; Tarnocai et al., 2009). The N amounts are linked strongly to plant species and biogeochemical processes, implying the nutrient status of peatlands has changed at different times during their Holocene development (Andersson et al., 2012). Rapid N sequestration in peatlands during the early Holocene might have contributed to the global decline in reactive N availability for terrestrial ecosystems, pointing to a significant but still undocumented role of northern peatlands in the global N cycle (McLauchlan et al., 2013). In addition, N availability is a major factor in controlling the plant growth needed for peat C accumulation (Olid et al., 2014). However, compared to peat C accumulation, little is known about long-term N accumulation in northern peatlands (Loisel et al., 2014). Therefore, better understanding of long-term peat N accumulation can also shed light on the responses of peatland development and peat C accumulation to global climate changes and help predict the future fate of peat C stocks in northern peatlands (Larsson et al., 2017).

The Altai Mountains in the arid and semi-arid region of northwest China have had a complex history of Holocene climate change due to their role as a topographic barrier and other local factors (hydrological condition, snowmelt water) (e.g., Wang & Zhang, 2019; Yang et al., 2019; Zhang & Feng, 2018; Zhang et al., 2016, 2018). As a start in contributing regional data and bridging knowledge gaps, the main objectives of this paper are (1) to describe the bulk properties of a peat sequence in the Altai Mountains of northwestern China and to emphasize the estimation and controls on Holocene peat C and N accumulation rates (CAR and NAR) in this special setting and (2) to identify differences in the magnitudes and the dynamics of long-term peat C and N accumulations under different climate control conditions in the Northern Hemisphere. This study would be useful for improved understanding of the responses of peat properties and long-term peat C and N accumulations and their controlling dynamics to climate changes and local factors under different ecologic-climatic scenarios.

2. Material and Methods

2.1. Regional Setting and Sample Collection

The Tielishahan (TLSH) peatland (48° 48′ 31″N, 86° 55′ 10″E, elevation ~1,770 m) is in an intermontane depression in the northernmost Altai Mountains, northwest China (Figure 1) and is situated ~7 km from the west Khanas National Nature Reserve of Xinjiang. This location is little influenced by human activities, and the peat sequence is therefore well preserved and provides a good geological archive for recording regional environment changes. The modern climate of the region has long cold winters that have perpetual snow and winter temperatures ranging from −12°C to −16°C. Summers are short, cool, and wet with temperatures less than 16°C. The mean annual temperature varies between −3.6°C and 1.8°C. The study site is in the temperate continental semi-arid climatic zone of central Asia with an annual precipitation of 500–600 mm, most
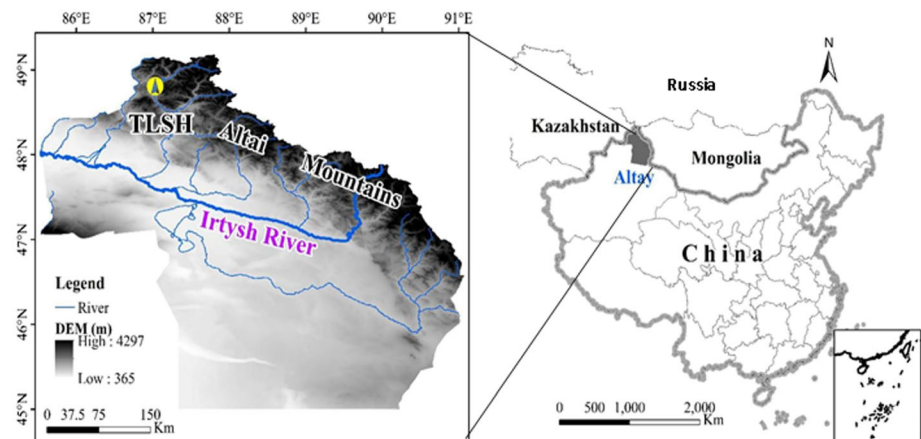
Figure 1. Location of the Tielishahan (TLSH) peatland and the study site in the Altai Mountains, northwestern China.

of which falls between June and August and is mainly delivered by the westerlies (Forestry Bureau of Altai Mountains in Xinjiang, 2003; Zhang et al., 2016, 2018).

The summer water depth of the surface peat to the top of the water table is 20–30 cm (measured in August 2014), with the water coming mainly from the combination of summer rainfall and surface runoff of glacier and snow meltwater. The plant communities around the peatland are coniferous forests dominated by larch (*Larix sibirica*) and spruce (*Picea obovata*) in higher elevations (>2,000 m asl), meadow steppe dominated by mixed grasses and sedges in the middle elevations (1,800–2,000 m asl), and desert vegetation in lower elevations (<1,800 m asl) (Zhang et al., 2018). The modern plant cover on the peat bog is dominated by *Carex* (*C. rhynchophysa*, *C. lasiocarpa*, and *C. pamirensis*), and *Sphagnum* (*S. palustre* and *S. rubellum*), and some *Polytrichum* sp. (Zhang et al., 2016). The regional climate features and the modern biomes in the surroundings of the peatland are described in more detail by Zhang et al. (2016, 2018).

A 400-cm sediment core was collected from the peatland using an Eijkelkamp peat sampler in August 2014. A 391-cm continuous peat layer constitutes most of the core, and gray lacustrine mud underlays the peat sequence (Figure 2). The peat layer is divided into eight parts by obvious differences in peat stratigraphy. Brown peat layers dominated by incomplete decomposition of stems and leaves of *Carex* spp. constitute the top 55 cm and the intervals at 150–193, 323–370, and 385–391 cm deeper in the sequence. The layers from 55 to 150 cm and from 370 to 385 cm are composed of light brown moss-peat with a mixture of *Carex* and *Sphagnum* remains. A yellow moss-peat layer with preserved moss residues is present from 193 to 218 cm, and then dark brown peat with a greater degree of decomposition and fewer *Carex* remains occupies the interval from 218 to 323 cm (Figure 2; Zhang et al., 2016, 2018).

2.2. Chronology of the Peat Sequence

The ^{14}C ages of five peat samples were determined by accelerator mass spectrometry (AMS) at the AMS laboratory of Peking University (Table 1). The dating samples were selected on the dual bases of the stratigraphic variations of the peat core and variations in the high resolution records of total organic matter (TOM) concentrations and humification degree (HD) of the whole peat sequence (Zhang et al., 2016). The more abundant *Carex* remains at the top of the core and apparent wood fragments at the bottom of the core provided plant macrofossil remains from 19 and 391 cm for ^{14}C dating. Because most peat samples contained insufficient macrofossil materials, three bulk peat samples at 100, 204, and 323 cm with roots removed were used for the ^{14}C dating (Table 1). At least 2.5-mg dry weight per sample was prepared for the AMS ^{14}C analysis. For the selected macrofossil samples, the peat was suspended in water and macrofossils were picked with forceps under a microscope for drying at 105°C. The bulk samples were analyzed in duplicate; the difference in ^{14}C age of each duplicate pair was less than 85 years. The radiocarbon ages were calibrated to calendar ages using CALIB Rev.7.0.1 software (Table 1). To establish chronology of the peat sequence, we used the Bayesian models that Blaauw et al. (2018) suggested are preferable to classical models, since their model assumptions produce more realistic reconstructions and better confidence intervals. In this study, we have improved the classical cubic-spline age-depth model that was tested by linear interpolation between
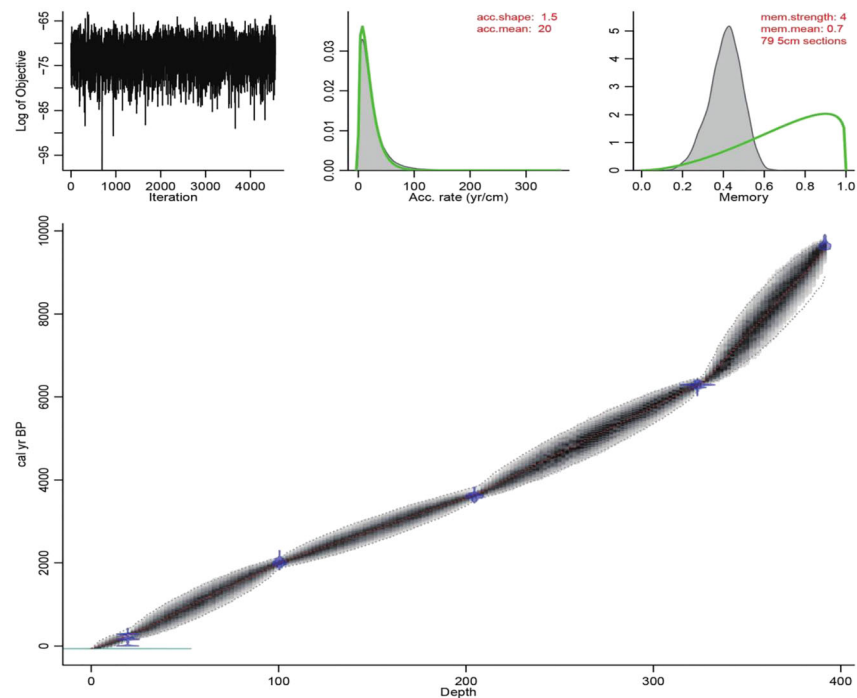
Figure 2. Age-depth model of the TLSH peat core. The blue symbols indicate actual data points, and the central dotted red line represents the "best" model based on the weighted mean age, while the outer gray dotted lines indicate 95% confidence interval. (For interpretation of the references to color in this figure legend, the reader is referred to the web version of this article.)

neighboring levels (Zhang et al., 2016, 2018) and replaced it with the "Bacon" package using the Bayesian approach (Blaauw et al., 2018; Blaauw & Christen, 2011) in the programming language R (R Core Team, 2015) (Figure 2 and Table 2).

2.3. Laboratory Analysis

Samples were taken at 2-cm intervals from the peat sequence for analysis of their bulk properties. A total of 196 peat samples was used for measurements of BD and loss on ignition (LOI), total organic carbon (TOC), and total nitrogen (TN), and stable C and N isotope compositions. The 1-cm^3 samples for BD analysis were dried overnight at 105°C and then combusted in a muffle furnace at 550°C for 4 h for determining the LOI values (Heiri et al., 2001). Separate samples for analysis of TOC, TN, and stable C and N isotopes were dried overnight at 105°C, cooled in a desiccator, and ground to <80 mesh. Dried bulk samples (0.1 g) were used for measuring TOC and TN concentrations using a CN-Analyzer (Vario MACRO cube, Elementar, Germany) with respective standard deviations of 0.5%. The TOC/TN molar ratios were calculated as TOC/12 ÷ TN/14. Dried bulk samples (5 mg) were used for determining peat C and N isotope compositions using a MAT 253 Isotopic Ratio Mass Spectrometer (Thermo Fisher Scientific, USA) and reported in their conventional δ notations (δ^{13}C and δ^{15}N). Stable carbon and nitrogen isotope results are expressed in parts per thousand

Table 1
AMS and Calibrated ^{14}C Age for the TLSH Peat Sequence in the Altai Mountains, Modified From Zhang et al. (2016, 2018)

Laboratory number[a]	Depth (cm)	δ^{13}C (‰)	Material dated	AMS^{14}C age (a BP)	Calibrated ^{14}C age (cal a BP)	Error age range (2σ)
BA-141084	19–20	−26.3	*Carex*	210 ± 30	150	0–305
BA-141085	100–101	−25.1	Bulk peat	2,045 ± 40	2010	1,900–2,120
BA-141086	204–205	−26.1	Bulk peat	3,365 ± 35	3,590	3,480–3,700
BA-141087	323–324	−26.3	Bulk peat	5,485 ± 35	6,300	6,200–6,400
BA-141088	391–392	−25.1	Wood	8,700 ± 40	9,710	9,540–9,880

[a]BA, accelerator mass spectrometry laboratory, Peking University.

Table 2
The Age-Depth Assignments Using Cubic-Spline Method and "Bacon" Package, Respectively

Depth (cm)	Age ranges (cal. a BP)	
	Cubic-spline age-depth model[a]	"Bacon" package age-depth model
0–20	0–180	−55 to 240
20–100	180–2,005	240–1,980
100–204	2,005–3,625	1,980–3,624
204–323	3,625–6,275	3,624–6,267
323–391	6,275–9,665	6,267–9,520

[a]Age-depth model that was used in previous publications (Zhang et al., 2016, 2018).

(‰) relative to the VPDB (Vienna PeeDee Belemnite) standard and air, respectively. Based on repeated standard measurements, $\delta^{13}C$ and $\delta^{15}N$ values were better than $\pm 0.15‰$.

Peat linear accumulation rates (PARs) in this study were re-estimated from the depth intervals and the corresponding calculated calendar ages derived from the Bayesian dating approach and are reported in cm/yr. CARs (g C/m^2/yr) and NARs (g N/m^2/yr) were calculated using TOC and TN concentrations, respectively, and the BD and PAR according to the following equation (Larsson et al., 2017):

$$X_{AR} = p \times b \times X \tag{1}$$

where X_{AR} is the CAR (g C/m^2/yr) or NAR (g N/m^2/yr), p is the PAR (m/yr), b is the dry BD (g/m^3), and X is the C or N concentration (g/g dry weight).

Pearson correlation analysis was used to test the correlations between peat proxies (BD, TOC, TN, TOC/TN, HD, $\delta^{13}C$, $\delta^{15}N$, and peat CAR and NAR, and PAR) (Table 3). The plant macrofossil data reported by Sun (2012) that reflect the compositions of Cyperaceae, *Sphagnum*, and moss communities in the TLSH peat core were used to interpret the relations between variations of dominant vegetation and changes in peat properties and peat CAR and NAR during the Holocene (Figures 4a and 4b).

3. Results

3.1. Peat Core Age-Depth Chronology

The calibrated age-depth relation model using the Bayesian approach indicates an age of ca. 10 kyr for the base of the core at 391 cm (Figure 2), which agrees well with the cubic-spline age-depth model that was used in previous publications (Zhang et al., 2016, 2018) and that indicated ca. 10 kyr BP for the onset of the transition from a paleolake to a peatland. The new Bayesian age scale indicates that the brown peat layer from 391 to 323 cm was deposited between 9.5 to 6.3 cal. kyr BP; the dark brown interval from 323 to 218 cm that is topped by a layer of yellowish peat corresponds to deposition between ca. 6.3 to 3.6 cal. kyr BP. The brown and yellow peat section from 218 to 100 cm was deposited from ca. 3.6 to 2 cal. kyr BP; the interval from 100 to 20 cm corresponds to deposition from ca. 2 to ~0.2 cal. kyr BP; and the top 20 cm of the core corresponds to the last ~200 cal. yr BP (Figures 2 and 3). As evident in Table 2, these age-depth assignments slightly differ in important ways from those reported in Zhang et al. (2016, 2018).

3.2. Peat Physicochemical Properties

High-resolution physicochemical measurements were made on samples taken at 2-cm intervals in the 391-cm peat core to identify changes that could be indicative of Holocene variations in the peat properties that affected peat accumulation at the TLSH site. The BD, LOI, TOC, and TN contents, TOC/TN ratios com-

Table 3
Pearson Correlation Analysis Between Peat Proxies (Bulk Density [BD], Total Organic Carbon [TOC], Total Nitrogen [TN], TOC/TN Molar Ratios, Humification Degree [HD], Bulk Peat ^{13}C Isotope, Bulk Peat $\delta^{15}N$ Isotope, and Carbon Accumulation Rate [CAR], Nitrogen Accumulation Rate [NAR], and Peat Accumulation Rate [PAR]) for TLSH Peat Sequence

	BD	TOC	TN	TOC/TN	HD	$\delta^{13}C$	$\delta^{15}N$	CAR	NAR	PAR
BD	1									
TOC	−0.261**	1								
TN	0.428**	0.012	1							
TOC/TN	−0.446**	0.278**	**−0.871****	1						
HD	0.631**	0.066	0.635**	**−0.534****	1					
$\delta^{13}C$	−0.519**	−0.072	−0.564**	0.484**	**−0.740****	1				
$\delta^{15}N$	0.470**	−0.271**	0.204**	−0.289**	0.398**	−0.375**	1			
CAR	0.071	0.288**	0.009	0.162	−0.037	0.170	−0.410**	1		
NAR	**0.820****	−0.079	**0.741****	**−0.667****	**0.805****	**−0.725****	0.516**	−0.135	1	
PAR	−0.539**	0.248**	−0.314**	0.397**	−0.495**	0.532**	**−0.599****	**0.764****	−0.643**	1

[a]*Note.* Statistically significant correlations are given in bold. **Represents *P* values < 0.01 (*n* = 196).
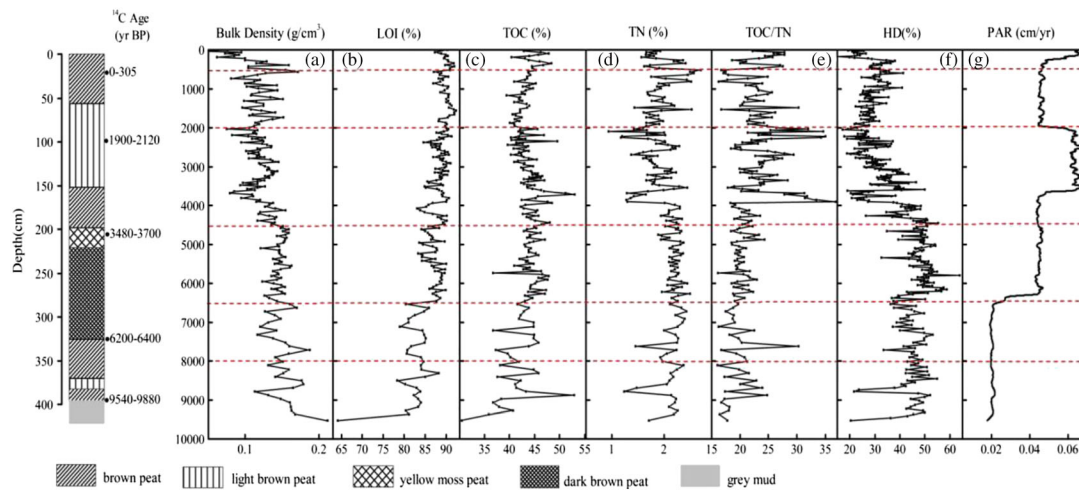
Figure 3. Peat stratigraphy and physicochemical records from TLSH peat sequence in the Altai Mountains, northwestern China: (a) bulk density, (b) loss-on-ignition (LOI), (c) total organic carbon (TOC) from Zhang et al. (2016), (d) total nitrogen (TN), (e) TOC/TN molar ratios, (f) humification degree (HD) from Zhang et al. (2016), and (g) peat accumulation rate (PAR). The diagram is divided into six time periods indicated by the red horizontal lines based on the variations in peat proxies.

pared to HD values, and PAR values of the peat sequence are shown in Figure 3. The TOC/TN molar ratios, organic $\delta^{13}C$ and total $\delta^{15}N$ values, and CAR and NAR values are compared to macrofossil evidence for plant assemblage changes at the site (Sun, 2012) in Figure 4.

3.2.1. Bulk Density and LOI

The BD values range from 0.05 to 0.23 g/cm³ in peat deposited over the 10-kyr record, with mean value of 0.13 ± 0.02 (SD) g/cm³ (Figure 3a). Higher values that average 0.16 ± 0.02 (SD) g/cm³ are found in the early Holocene before 8 cal. kyr BP, and then the values fluctuate around a mean of 0.14 ± 0.01 (SD) g/cm³ in the peat layers deposited in the middle Holocene from 8 to 4.5 cal. kyr BP. Lower values with a mean of 0.11 ± 0.01 (SD) g/cm³ occur from 4.5 to 2 cal. kyr BP; and then the values increase to a mean value of 0.12 ± 0.02 (SD) g/cm³ between 2 to 0.5 cal. kyr BP. The lowest bulk density values occur in the peat deposited during the last 500 years.

LOI is a parameter for reflecting total organic matter (TOM) content of the peat. The LOI values range from 64% to 94% over the whole peat core, with mean values of $87.6 \pm 3.3\%$ (SD). Relatively lower values appear
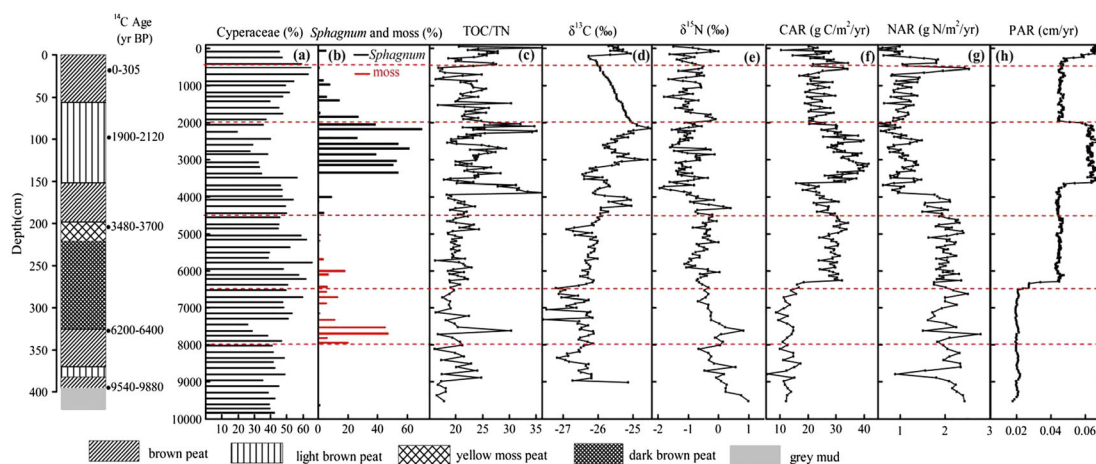

Figure 4. Proportions of (a) Cyperaceae and (b) *Sphagnum* and moss macrofossils (Sun, 2012), (c) TOC/TN ratios, (d) bulk peat ¹³C isotope, (e) bulk peat ¹⁵N isotope, (f) carbon accumulation rate (CAR), and (g) nitrogen accumulation rate (NAR). The diagram is divided into six time periods indicated by the red horizontal lines based on the variations in peat isotope proxies, plant macrofossils and peat CAR, NAR, and PAR.

before 6.5 cal. kyr BP, then they increase from 6.5 cal. kyr BP, and higher values that fluctuate narrowly between 83% and 90% occur from 6.5 to 2 cal. kyr BP. The highest LOI content (~92%) appears during the last 2 cal. kyr BP (Figure 3b).

3.2.2. TOC and TN Concentrations and TOC/TN Ratios

TOC concentrations vary between 30% and 54%, and TN concentrations range from 0.8% to 2.7% over the whole peat sequence, with mean values of $43.6 \pm 2.8\%$ (SD) and $2.0 \pm 0.3\%$ (SD), respectively (Figures 3c and 3d). The early and middle Holocene sections from 10 to 6.5 cal. kyr BP exhibit lower TOC concentrations with a mean value of $41.5 \pm 3.9\%$ (SD). Stable TOC concentrations with a mean value of $44.5 \pm 1.9\%$ (SD) occur from 6.5 to 4.5 cal. kyr BP, and then the values decrease slightly to $43.9 \pm 2.4\%$ (SD) from 4.5 to 2 cal. kyr BP before increasing again after 2 cal. kyr BP (Figure 4c). TN concentration in the peat sequence remains higher and uniform (~$2.2 \pm 2.4\%$ [SD]) before 4.5 cal. kyr BP, except for the lower values at two transient times (ca. 9 cal. kyr BP and 7.5 cal. kyr BP). The lowest values (~0.8%) occur between 4.5 and 2 cal. kyr BP before increasing gradually to their maxima (2.7%) during the last 2 cal. kyr BP (Figure 3d). The molar TOC/TN ratios in the peat sequence range widely from 15.2 to 35.1, with a mean value of 22.2 ± 4.0 (SD) The mean ratio is lower (19.9 ± 2.2 [SD]) during the early and middle Holocene before 4.5 cal. kyr BP, and then ratios increase to their maximum but with major fluctuations from 4.5 to 2 cal. kyr BP. Then they decrease slightly to the lowest value at ca. 0.5 cal. kyr BP and increase again during the last 0.5 cal. kyr BP. The variations in TOC/TN ratios have a close relation with peat HD values in the TLSH setting (Figures 3e and 3f).

3.2.3. PAR Associated With Improved Age-Depth Model

Based on the improved age-depth model using the Bayesian approach, PAR was very slow (0.02 ± 0.001 [SD] cm/yr) before 6.5 cal. kyr BP and increased to 0.04 ± 0.003 (SD) cm/yr from 6.5 to 4 cal. kyr BP. The maximum (~0.67 cm/yr) occurred between 4 and 2 cal. kyr BP, and the values decreased to 0.04 ± 0.007 (SD) cm/yr again from 2 to 0.5 cal. kyr BP. Accumulation again increased from 0.5 cal. kyr BP to the present (Figure 3g). This variation is slightly different from the previous study using a cubic-spline age-depth model that recorded that the PAR was initially slow and increasing from 4 to 2.5 cal. kyr BP, and accumulation was again slow after 2.5 cal. kyr BP before increasing rapidly to the maximum during the last 1 cal. kyr BP (Zhang et al., 2016).

3.2.4. Organic δ^{13}C and Total δ^{15}N Values

The δ^{13}C values in the TLSH peat sequence range between −27.6‰ and −24.5‰, and the δ^{15}N values range from −2.0‰ to 1.0 ‰, with mean values of -25.9 ± 0.6‰ (SD) and -0.7 ± 0.52‰ (SD), respectively (Figures 4d and 4e). Except for the very bottom sample that has a value of about −25‰, δ^{13}C values are lower in the early Holocene sediments deposited before 6.5 cal. kyr BP with mean value of -26.5 ± 0.4 ‰ (SD); then the values increase gradually and reach their maxima at ca. 2 cal. kyr BP. Notable decreases in the δ^{13}C values appear since 2 cal. kyr BP, except for the uppermost peat layers that correspond to the last 500 cal. yr BP (Figure 4d). Total δ^{15}N values are higher (0.43 ± 0.4‰ [SD]) before 8 cal. kyr BP, but they decrease slightly from 8 to 4.5 cal. kyr BP. The values decrease rapidly and have more negative values (a mean value of -1.0 ± 0.4‰ [SD]) since 4.5 cal. kyr BP (Figure 4e).

3.2.5. CAR and NAR Variations

The CARs share variations with the peat PAR values and vary widely between 5.3 to 41.7 g C/m^2/yr, with a mean value of 25.4 ± 7.7 (BD) g C/m^2/yr over the whole peat sequence (Figures 4f and 4h). CAR is lower in the early Holocene peat with the mean value of 12.6 ± 2.3 (SD) g C/m^2/yr, then it increases to ~29.5 g C/m^2/yr from 6.5 to 4.5 cal. kyr BP, and the highest value appears in the period between 4.5 and 2 cal. kyr BP. The CAR then decreases to ~25.5 g C/m^2/yr after 2 cal. kyr BP. The NARs vary between 0.5 and 3.2 g N/m^2/yr, with a mean value of 1.5 ± 0.5 (SD) g N/m^2/yr (Figure 4g). Unlike the CARs, the variations of NARs do not coincide with the PARs and instead have a higher mean value of 2.1 ± 0.5 (SD) g N/m^2/yr before 4.5 cal. kyr BP before decreasing rapidly to the lowest value between 4.5 to 0 cal. kyr BP.

4. Discussion

4.1. Peat Properties and Peat C and N Accumulations in the Altai Mountains, Northwestern China

4.1.1. Holocene Changes in Peat Properties

Patterns of decreasing BD and increasing LOI and TOC (Figures 3a–3c) represent an increase in the OM input to the TLSH peatland over the Holocene. The variations result most likely from smaller organic material inputs during the early stage of peatland development and greater contributions from plants with higher
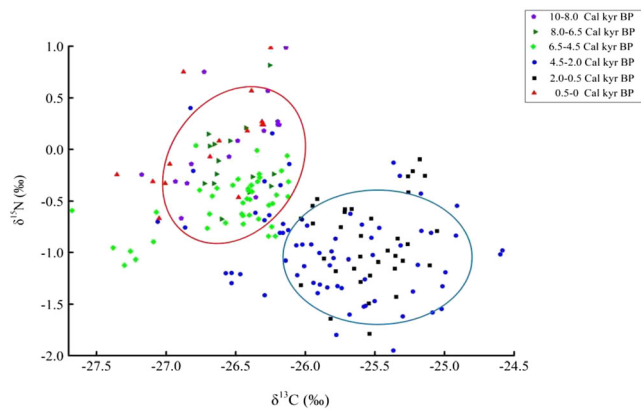
Figure 5. Contributions of plant types in different periods during the Holocene and their relations with peat $\delta^{13}C_{organic}$ (‰) and $\delta^{15}N_{total}$ (‰). The red ellipses represent peat samples during the period dominated by vascular plants; the blue ellipses represent peat samples during the late Holocene from 4.5 to 0.5 cal. kyr BP when *Sphagnum* spp. became important.

OM since 6.5 cal. kyr BP (Feng et al., 2017; Zhang et al., 2018), as well as from continuing decomposition and subsequent compaction of peat over time (Loisel et al., 2014). TOC/TN ratios correlate negatively with peat TN concentration ($r = -0.871$, $P < 0.01$) and peat HD values ($r = -0.534$, $P < 0.01$) (Table 3 and Figures 3d–3f), which indicate that changes in TN concentration and degree of peat decomposition related closely to local conditions have an important impact on TOC/TN ratios in the peatland.

Differences in peat bulk properties largely reflect changes in peat vegetation types (Andersson et al., 2012; Larsson et al., 2017; Loisel et al., 2014). Non-*Sphagnum* peat is characterized by higher BD, higher C and N contents, and lower OM content and TOC/TN ratios than samples composed of *Sphagnum*-dominated peat, which is more resistant to decomposition and preferentially accumulates in peat, leading to higher PARs in bogs as opposed to fens dominated by herbaceous plants (Andersson et al., 2012; Loisel et al., 2014). This factor is evident in the TLSH sequence, which records that peat bulk properties are associated with Holocene changes in dominant peat-forming plants as indicated by plant macrofossil records reported by Sun (2012) (Figures 4a and 4b). Lower BD, TOC, and TN contents and higher LOI and TOC/TN ratios between 4.5 and 2 cal. kyr BP are related to the peat samples dominated by *Sphagnum* spp. that contributed to the highest PAR values. An opposing trend in these values occurs in other intervals and is related to *Carex*-dominated peat that experienced greater degradation, especially in the interval before 4.5 cal. kyr BP. However, the notably lower BD and higher values in LOI, TOC, and TN concentrations and in TOC/TN ratios during the last 500 cal. yr BP (Figures 3, 4a, and 4b) are most likely related to abundant modern *Carex* input and a shorter time for degradation.

Peat $\delta^{13}C$ values in the TLSH peat sequence negatively correlate strongly with peat HD values ($r = -0.740$, $P < 0.01$), and $\delta^{15}N$ values have negative correlations with PAR ($r = -0.599$, $P < 0.01$) (Table 3). More negative $\delta^{13}C$ values (less than $-26‰$) and higher peat $\delta^{15}N$ values (larger than ~ $-0.5‰$) are associated with a dominance of vascular plants and correlate with higher HD values but lower PARs that relate to a high degree of decomposition before 4.5 cal. kyr BP, whereas the late Holocene intervals after 4.5 cal. kyr BP that are dominated by *Sphagnum* spp. correlate with lower HD values but higher PARs and exhibit less negative $\delta^{13}C$ values and more negative peat $\delta^{15}N$ values (Figure 3f, 4, and 5). Therefore, we find that peat-forming plants and peat decomposition rates are major factors in determining peat C and N isotopic compositions in the Altai Mountains. This relation is supported by other studies that found the C and N isotopic compositions of peat can reflect conditions at the time of assimilation of C and N and also peat decay processes, which are both related closely to the types of peat-forming plants and to local condition (e.g., Andersson et al., 2012; Biester et al., 2014; Larsson et al., 2017). In general, more negative $\delta^{13}C$ values in the peat are associated with vascular plant remains, suggesting that greater ^{13}C depletion occurs during the decomposition that is generally more extensive in peatlands dominated by vascular plants than in those dominated by *Sphagnum* spp. (Andersson et al., 2012; Larsson et al., 2017). The enrichment of ^{15}N in peat could also be a consequence of the isotope-sensitive N recycling that is associated with peat decomposition. The decomposition process likely leads to preferential loss of ^{14}N from the bulk peat, leaving the N remaining in the peat enriched in [15]N (Andersson et al., 2012; Larsson et al., 2017).

4.1.2. Regional Comparison of the Peat Properties

Differences in peat properties exist between regions due to the different peat types and sample ages (Loisel et al., 2014). The TLSH peatland, located in an intermontane depression in northwestern China, has accumulated from a mixed group with *Carex* and *Sphagnum* spp. over the Holocene (Sun, 2012; Figures 4a and 4b). Compared to other regions (Table 4), the TLSH peat has slightly lower BD but higher OM and C values than the Hani peat in northeastern China (Cai et al., 2013) and the peat in two sequences on the Tibetan Plateau, where both peatlands are dominated by sedges (H. Chen et al., 2014). However, the TLSH BD values are higher and OM and C contents are lower than those in most peatlands in northern Europe regions, where peatlands are mostly composed of herbaceous, humified, and brown moss types

Table 4
Summary Table of Mean Values of Peat Properties in Northern Peatlands in Different Regions, Along With the Number of Samples (n)

	Northwestern China (this study)	Tibetan plateau[a,b]	Northeastern China[c,d]	Western Canada[e]	Eastern Canada[e]	Continental Europe[e]	Western Russia[e]	Circum-Arctic[e]
Bulk density(g/cm³)	0.128 ± 0.02 (n = 196)	0.201–0.489[a]	0.136	0.166 ± 0.07 (n = 3,635)	0.100 ± 0.04 (n = 2,834)	0.120 ± 0.14 (n = 410)	0.118 ± 0.07 (n = 2,701)	0.118 ± 0.07 (n = 21,220)
Organic matter content (%)	87.6 ± 3.3 (n = 196)	72.5	62.2	91.6 ± 8.1 (n = 3,442)	97.8 ± 6.5 (n = 1835)	97.4 ± 5.4 (n = 305)	94.6 ± 10.3 (n = 2,666)	90.7 ± 13 (n = 18,973)
Total carbon content (%)	43.6 ± 2.8 (n = 196)	38.4	36.1	45.0 ± 4.3 (n = 382)	48.9 ± 3.7 (n = 1,084)	38.9 ± 1.3 (n = 60)	49.2 ± 3.2 (n = 74)	49.2 ± 2.4 (n = 21,220)
Total nitrogen content (%)	1.99 ± 0.3 (n = 196)	2.1	1.2	1.1 ± 0.8 (n = 265)	0.9 ± 0.5 (n = 1,084)	0.7 ± 0.1 (n = 60)	1.6 ± 0.9 (n = 44)	1.2 ± 0.7 (n = 3,365)
C/N ratio	22.2 ± 4.0 (n = 196)	14.08–111	—	62.4 ± 0.37.5 (n = 265)	77.2 ± 56.1 (n = 1,084)	54.2 ± 7.6 (n = 60)	40.8 ± 21.7 (n = 44)	55 ± 33 (n = 3,326)

[a]Large et al. (2009). [b]H. Chen et al. (2014). [c]Cai et al. (2013). [d]Leng et al. (2003). [e]Loisel et al. (2014).

(Loisel et al., 2014). It is notable that higher N concentrations and significantly lower C/N ratios occur in the TLSH peat than in most other northern peatlands (Table 4), reflecting a higher degree of peat decomposition in the Altai Mountains. Overall, peat properties in the Altai Mountains in northwest China exhibit differences from those in most other northern peatlands, probably because of differences in peat-forming plant communities and the degrees of decomposition between different regions.

4.1.3. Variations in Long-Term Peat C and N Accumulations in the Altai Mountains

Changes in primary productivity controlled by regional climate conditions are a major controller of variations in peat C accumulation in many regions (e.g., Charman et al., 2013; Xing et al., 2015). The TLSH peat sequence exhibits variations in Holocene CARs that have significant correlations ($r = 0.764$, $P < 0.01$) with changes in PAR during different intervals (Table 3 and Figures 4f and 4h). The lowest CAR values (12.6 ± 2.3 (SD) g C/m²/yr), which coincide with the lowest PAR values before 6.5 cal. kyr BP (Figures 4f and 4h), might be the consequence of lower productivity and greater peat decomposition during the early stage of the transition from a lake setting to a peatland (Feng et al., 2017; Zhang et al., 2018). A classic fen ecosystem with higher productivity dominated by a Cyperaceae community was not established until after 6.5 cal. kyr BP (Zhang et al., 2016, 2018), and a higher CAR (28.6 ± 3.7 (SD) g C/m²/yr) accompanied the increase in vertical peat growth from 6.5 cal. kyr BP (Figures 4f and 4h).
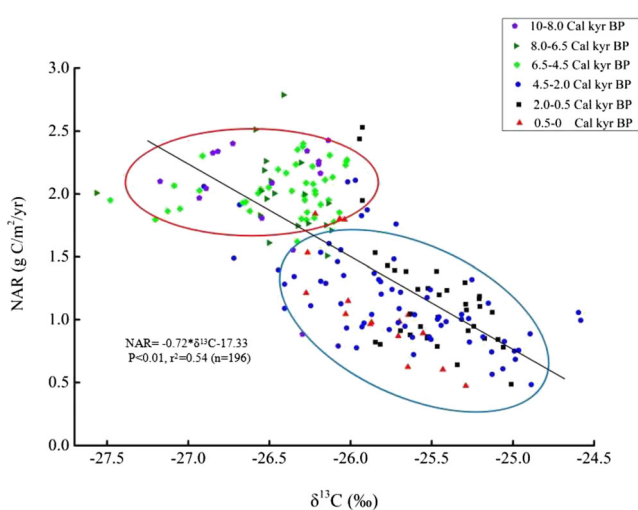
The significantly highest CAR (30.5 ± 6.0 (SD) g C/m²/yr) in the interval between 4.5 and 2 cal. kyr BP coincides with a shift in the dominant vegetation from a Cyperaceae community to *Sphagnum* species that are more resistant to decomposition and preferentially accumulate in the peat (Figures 4a, 4b, 4f, and 4h). In addition, the co-occurrence of vascular plants and *Sphagnum* spp. could contribute to higher productivity, as the vascular plant residues may act as a supporting structure for *Sphagnum* spp. and may also contribute more litter to make a thicker acrotelm (Larsson et al., 2017; Malmer et al., 1994; Moore et al., 2002; Wallén & Malmer, 1992). Also, higher peat CAR values could also result from wetter conditions, which would contribute to a shorter residence time of biomass in the aerobic acrotelm (Loisel & Garneau, 2010). Therefore, we postulate that the major factors resulting in higher CARs from 4.5 and 2 cal. kyr BP might be the higher moss productivity associated with co-occurrence of vascular plants and *Sphagnum* spp. and the wetter conditions that favor less peat decomposition (Sun, 2012; Zhang et al., 2016). After 2 cal. kyr BP, the contribution of *Sphagnum* spp. decreased sharply, and vascular plants became dominant (Sun, 2012; Figures 4a and 4b), causing lower CARs and PARs than the preceding interval but at the same level as between 6.5 and 4.5 cal. kyr BP when the peatland was also dominated by vascular plants (Figures 4f and 4h).
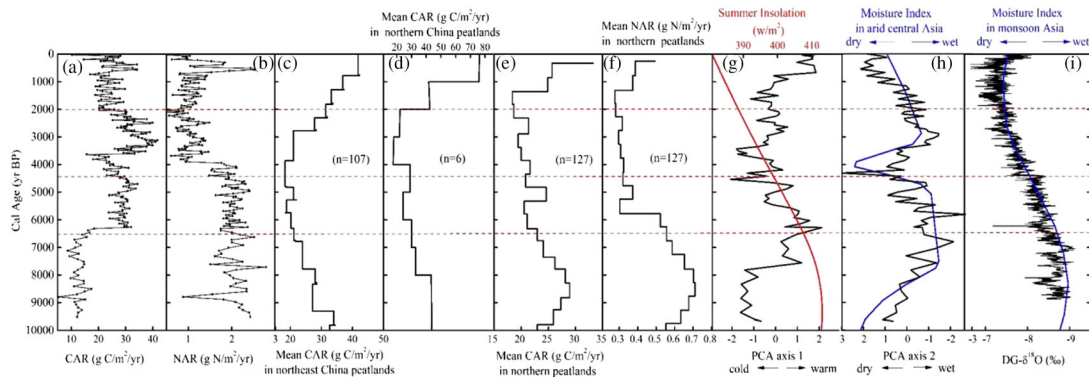

Figure 6. Relations between nitrogen accumulation rates (NAR) and $\delta^{13}C_{organic}$ (‰). The red ellipses represent peat samples during the period before 4.5 cal. kyr BP dominated by vascular plants; the blue ellipses represent peat samples after 4.5 cal. kyr BP when *Sphagnum* spp. became important.

Figure 7. Holocene peat (a) carbon and (b) nitrogen accumulation rates (CAR and NAR) in the TLSH Altai Mountains peatland in northwest China (our study), (c) mean Holocene peat carbon accumulation rate record from peatlands ($n = 107$) in northeast China (Xing et al., 2015), (d) mean Holocene peat carbon accumulation rate from peatlands ($n = 6$) in other northern China locations (Zhao et al., 2014), (e) mean Holocene peat carbon accumulation rate from peatlands ($n = 127$) in northern peatlands (Loisel et al., 2014), (f) mean Holocene peat nitrogen accumulation rate from peatlands ($n = 127$) in northern peatlands (Loisel et al., 2014), (g) pollen-based temperature (PCA axis1) reconstructions in Altai Mountains (Zhang et al., 2018) and July insolation at 65°N (red curve) in the Northern Hemisphere during the Holocene (Berger & Loutre, 1991), (h) pollen-based moisture (PCA axis 1) reconstructions in the Altai Mountains (Zhang et al., 2018) and Holocene moisture index in arid central Asia (blue curve) modified by F. H. Chen et al. (2016), and (i) stalagmite $\delta^{18}O$ values of the Dongge Cave (DG) (Wang et al., 2005) and Holocene moisture index in monsoon China (blue curve) from Zhao et al. (2009). The diagram is divided into four time periods indicated by the red horizontal lines based on the variations in peat CARs and climate indices in different regions.

Holocene NARs in the TLSH peat sequence are strongly correlated with the variations in peat BD values ($r = 0.820$, $P < 0.01$) and peat TN contents ($r = 0.741$, $P < 0.01$) (Table 3). Moreover, a strong correlation between NAR and $\delta^{13}C$ ($r = -0.725$, $P < 0.01$) reveals that less negative $\delta^{13}C$ values (larger than $-26‰$) in peat deposited before 4.5 cal. kyr BP are associated with markedly higher NARs (2.0 ± 0.3 (SD) g N/m^2/yr) in peat that was dominated by vascular plants, whereas more negative $\delta^{13}C$ values during the intervals after 4.5 cal. kyr BP are associated with *Sphagnum* remains and lower NARs (1.1 ± 0.4 (SD) g N/m^2/yr) (Table 3 and Figure 6). Although the PAR reaches its maximum in the interval from 4.5 and 2 cal. kyr BP, the lowest NAR coincides with the *Sphagnum*-dominance in the peat that contributes to lower peat BD and lower TN contents (Figures 4b, 4g, and 4h).

In addition, the TLSH peat sequence also has variations in Holocene NARs that correlate with changes in the peat TOC/TN ratio ($r = -0.667$, $P < 0.01$) and peat HD ($r = 0.805$, $P < 0.01$) that are both associated closely with the degree of peat decomposition (Table 3). A high degree of decomposition, indicated by lower TOC/TN ratios and higher peat HD values, contributes to higher NARs before 4.5 cal. kyr BP, whereas slower decomposition after 4.5 cal. kyr BP might have caused the decreases in peat NAR (Figures 3 and 4). We therefore postulate that changes in both the dominant plant types in the peatland and the degree of peat decomposition that releases N for plant primary production have played important roles in determining long-term N accumulations in the Altai Mountains during the Holocene. Moreover, the slower decomposition rate of the *Sphagnum* OM can retard N recycling, thereby limiting the availability of this essential nutrient to vascular plants and leading to lower NAR values.

4.2. Possible Controls on Holocene C and N Accumulation in Peat in Northwest China
4.2.1. Regional Comparison and Possible Controls on C Accumulation in Peat

Holocene CARs in the TLSH peatland from the Altai Mountains of northwest China vary from 5.3 to 41.7 g C/m^2/yr (mean 25.4 ± 7.7 (SD) g C/m^2/yr) (Figure 7a). These rates are slightly higher than the Holocene mean CAR values of 22.9 ± 2.0 (SD) g C/m^2/yr and 18.6 g C/m^2/yr in Northern Hemisphere peatlands estimated by Loisel et al. (2014) and Yu et al. (2009), respectively. However, the mean CAR at the TLSH setting is lower than that in monsoonal regions of northern China, which have a mean CAR value of 37.7 g C/m^2/yr in northeast China (Figure 7c, Xing et al., 2015) and 40.2 g C/m^2/yr in other Chinese locations (Figure 7d, Zhao et al., 2014). CARs in other northern peatlands generally show high values in the early and middle Holocene and then decrease during the middle and late Holocene (Figures 7c–7e). However, unlike the variations of Holocene C accumulations in most peatlands, the Altai Mountains peatland has lower CAR values (mean 12.7 ± 2.4 (SD) g C/m^2/yr) in the early and middle Holocene before 6.5 cal. kyr

BP that is followed by an increase to a maximum in the late Holocene from 6.5 to 2 cal. kyr BP and then a rapid decrease since 2 cal. kyr BP (Figures 7a and 7c–7e).

In general, climate acts as the key driver of CAR in northern peatlands; warmer and wetter climate can stimulate plant growth and accelerate peat accumulation and reduce its decay (Charman et al., 2013; Panait et al., 2017; Yu et al., 2010). Higher CARs during the early and middle Holocene are associated with higher primary production and decreased decomposition caused by higher summer insolation and stronger seasonality (e.g., Loisel et al., 2014; Yu et al., 2010; Zhao et al., 2014). In monsoonal China, higher C accumulation during the Holocene might be attributed to higher productivity related to both higher temperatures and the optimal moisture provided by stronger monsoon intensity (Xing et al., 2015; Zhao et al., 2014). At a local scale, other factors, such as plant community composition, local water levels, nutrient availability, topography, and human disturbance, also play important roles in controlling peat C accumulation (Charman et al., 2012, 2015; Panait et al., 2017). In the Altai Mountains, the cold-dry climate pattern caused by both the melting of ice sheets related to stronger summer insolation and the weakened westerlies during the early Holocene is not consistent with the early Holocene warmer and wetter climate in monsoonal Asia that was related to stronger monsoon intensity (Figures 7f–7h; Zhang et al., 2018). The TLSH setting transitioned from a lake to a peatland during the early Holocene, when lower productivity with limited vascular plant inputs constrained peat accumulation. We therefore speculate that lower peat CARs in the Altai Mountains region during the early Holocene might be attributed to both cold-dry climate and changes in local hydrological conditions that led to limited development of vascular land plants and consequent lower productivity (Feng et al., 2017; Zhang et al., 2018).

Lower values of long-term peat C accumulation in global northern peatlands from 6.5 to 2 cal. kyr BP (Figure 7e, Loisel et al., 2014) coincided with the onset of the Neoglacial cooling interval that was characterized by a colder climate that reduced the peat C-sink capacity (Jones & Yu, 2010; Loisel et al., 2014). Decreased summer insolation and diminished monsoon intensity also contributed to lower peat CAR values in Asian monsoonal regions (Figures 7c, 7d, and 7i). A long interval of significantly warmer and wetter climate that occurred in the Altai Mountains from 6.5 to 2.0 cal. kyr BP (Figures 7g and 7h) stimulated more primary production with a higher nutrient availability in the peatland, which probably was the major contributor to higher peat CAR (Figure 7a). Finally, the highest CAR, from 4.5 to 2 cal. kyr BP, is attributed principally to establishment of a typical *Sphagnum*-dominated bog during wetter conditions (Sun, 2012; Figure 4h and 7a). Unlike the increasing C accumulations in monsoonal regions during the warm and wet late Holocene related to a strong East Asia summer monsoon that stimulated primary production (Loisel et al., 2014; Xing et al., 2015; Yu et al., 2009; Zhao et al., 2014), decreased peat CAR values in the TLSH peatland during the late Holocene could be ascribed to drier conditions with lower productivity and a higher degree of peat decomposition that restricted peat accumulation, when arid central Asia entered an interval of dry climate with diminished delivery of moisture by the weakened westerlies since 2 cal. kyr BP (Figure 7h; Zhang et al., 2018).

4.2.2. Possible Controls on N Accumulation in Peat

Relative to the many studies that have reported the accumulation of C in peatlands during the Holocene, the accumulation of N has received far less attention. A synthesis of the limited number of studies reported that the long-term rates of N accumulation in northern peatlands averages 0.5 g N/m^2/yr, with the early Holocene having an NAR of 0.61 g N/m^2/yr and the middle and late Holocene since 6 cal. kyr BP having an average value of 0.34 g N/m^2/yr (Figure 7f, Loisel et al., 2014). In the Altai Mountains, the Holocene peat NAR ranges from 0.5 to 2.8 g N/m^2/yr and averages 1.5 ± 0.5 (SD) g N/m^2/yr, or about 3 times higher than the mean rate in other northern peatlands, and the early and middle Holocene before 4.5 cal. kyr BP has even higher rates (~2.0 g N/m^2/yr). The lowest values (~0.5 g N/m^2/yr) that are equivalent to the average global rate appear only after 4.5 cal. kyr BP (Figures 7b and 7f). In general, the Holocene N accumulation trend mirrors that of C accumulation in peatlands, and both are influenced by peat density and PARs (Figures 7e and 7f; Loisel et al., 2014). However, the TLSH peat NAR variations differ from peat CAR variations during the Holocene (Figures 7a and 7b). The changes in CARs have close relations with the PARs, whereas the peat NARs share variations corresponding to peat BD, TN, and TOC/TN ratios, which are closely related to peat decomposition and dominance of either Cyperaceae or *Sphagnum* plants (Table 3 and Figures 3 and 4). The lowest NARs during the interval from 4.5 to 2 cal. kyr BP are associated with lower peat density, lower N content, and higher TOC/TN ratios in this time when the peatland was dominated by

Sphagnum spp. (Figures 4b and 7b). This finding is in line with the peat N accumulation results in other northern peatlands that are described by Loisel et al. (2014) and Larsson et al. (2017), who point out that the increasing presence and persistence of *Sphagnum* is the major factor for low NARs during the middle and late Holocene in northern peatlands (Figure 7f). Similarly, we can attribute higher NARs before 4.5 cal. kyr BP to the *Carex* dominance that produced peat with higher N contents and lower TOC/TN ratios that relate to greater peat decomposition and a relatively higher release of N to stimulate plant primary production (Figures 4b and 7f).

5. Conclusion

Holocene changes in peat properties demonstrate that shifts in peat properties in the Altai Mountains are related closely to changes in peat-forming plants and degree of decomposition. *Sphagnum*-dominated peat (4.5–2 cal. kyr BP) that is relatively resistant to decomposition contributed to notably lower BD, TOC, and TN contents and peat δ^{15}N values and higher LOI, TOC/TN ratios and peat δ^{13}C values. These indicators of peat properties show opposite changes in other intervals that relate to *Carex*-dominated peat and its greater susceptibility to degradation. Unlike other northern peatlands, the Holocene peat C accumulation in the Altai Mountains of northwest China shows lower rates during the early and middle Holocene and higher CARs during the late Holocene, coinciding with changes in PARs. The NAR variations resemble those in other northern peatlands, which had higher rates during the early and middle Holocene and had lower rates during late Holocene, corresponding to changes in peat BD, TN, and TOC/TN ratios. Regional Holocene climate changes controlled by the westerlies and changes in local plant types and peat decomposition evidently played important roles in determining long-term peat CARs and NARs in the rugged Altai Mountains of northwest China.

Data Availability Statement

The analytical data on which this contribution is based are available at https://doi.org/10.7302/3srj-pr33 at Deep Blue Data Repository.

References

Andersson, R. A., Meyers, P., Hornibrook, E., Kuhry, P., & Mörth, C. M. (2012). Elemental and isotopic carbon and nitrogen records of organic matter accumulation in a Holocene permafrost peat sequence in the East European Russian Arctic. *Journal of Quaternary Science*, *27*, 545–552.

Berger, A., & Loutre, M. F. (1991). Insolation values for the climate of the last 10 million years. *Quaternary Science Reviews*, *10*(4), 297–317. https://doi.org/10.1016/0277-3791(91)90033-Q

Biester, H., Knorr, K. H., Schellekens, J., Basler, A., & Hermanns, Y. M. (2014). Comparison of different methods to determine the degree of peat decomposition in peat bogs. *Biogeosciences*, *11*(10), 2691–2707. https://doi.org/10.5194/bg-11-2691-2014

Blaauw, M., & Christen, J. A. (2011). Flexible paleoclimate age-depth models using an autoregressive gamma process. *Bayesian Analysis*, *6*, 457–474.

Blaauw, M., Christen, J. A., Bennett, K. D., & Reimer, P. J. (2018). Double the dates and go for Bayes—Impacts of model choice, dating density and quality on chronologies. *Quaternary Science Reviews*, *188*, 58–66. https://doi.org/10.1016/j.quascirev.2018.03.032

Cai, C., Hong, B., Zhu, Y. X., Hong, Y. T., Wang, Y., & Peng, H. J. (2013). Holocene Peat carbon accumulation rates and influence factors from the Hani peatland, Northeast China. *Earth and Environment*, *41*, 597–604. (In Chinese)

Charman, D. J., Amesbury, M. J., Hinchliffe, W., Hughes, P. D., Mallon, G., Blake, W. H., & Mauquoy, D. (2015). Drivers of Holocene peatland carbon accumulation across a climate gradient in northeastern North America. *Quaternary Science Reviews*, *121*, 110–119. https://doi.org/10.1016/j.quascirev.2015.05.012

Charman, D. J., Beilman, D. W., & Blaauw, M. (2013). Climate-related changes in peatland carbon accumulation during the last millennium. *Biogeosciences*, *10*(2), 929–944. https://doi.org/10.5194/bg-10-929-2013

Charman, D. J., Hohl, V., Blundell, A., Mitchell, F., Newberry, J., & Oksanen, P. (2012). A 1000-year reconstruction of summer precipitation from Ireland: Calibration of a peat-based palaeoclimate record. *Quaternary International*, *268*, 87–97. https://doi.org/10.1016/j.quaint.2011.12.011

Chen, F. H., Jia, J., Chen, J. H., Li, G. Q., Zhang, X. J., Xie, H. C., et al. (2016). A persistent Holocene wetting trend in arid central Asia, with wettest conditions in the lake Holocene, revealed by multi-proxy analyses of loess-paleosol sequences in Xinjiang, China. *Quaternary Science Reviews*, *146*, 134–146. https://doi.org/10.1016/j.quascirev.2016.06.002

Chen, H., Yang, G., Peng, C., Zhang, Y., Zhu, D., Zhu, Q., et al. (2014). The carbon stock of alpine peatlands on the Qinghai-Tibetan Plateau during the Holocene and their future fate. *Quaternary Science Reviews*, *95*, 151–158. https://doi.org/10.1016/j.quascirev.2014.05.003

Core Team, R. (2015). *R: A language and environment for statistical computing*. Vienna, Austria: Foundation for Statistical Computing. https://www.R-project.org/

Feng, Z. D., Sun, A. Z., Abdusalih, N., Ran, M., Kurban, A., Lan, B., et al. (2017). Vegetation changes and associated climatic changes in the southern Altai Mountains within China during the Holocene. *The Holocene*, *27*(5), 683–693. https://doi.org/10.1177/0959683616670469

Forestry Bureau of Altai Mountains in Xinjiang (2003). Two-river source comprehensive scientific investigation of Altai Mountains in Xinjing, Urumchi. (in Chinese).

Gorham, E. (1991). Northern peatlands: Role in the carbon cycle and probable responses to climatic warming. *Ecological Applications*, *1*(2), 182–195. https://doi.org/10.2307/1941811

Heiri, O., Lotter, A. F., & Lemcke, G. (2001). Loss on ignition as a method for estimating organic and carbonate content in sediments: Reproducibility and comparability of results. *Journal of Paleolimnology*, *25*(1), 101–110. https://doi.org/10.1023/A:1008119611481

Jones, M. C., & Yu, Z. (2010). Rapid deglacial and early Holocene expansion of peatlands in Alaska. *Proceedings of the National Academy of Sciences USA*, *107*, 7347–7352.

Lacourse, T., & Davies, M. A. (2015). A multi-proxy peat study of Holocene vegetation history, bog development, and carbon accumulation on northern Vancouver Island, Pacific coast of Canada. *The Holocene*, *25*(7), 1165–1178. https://doi.org/10.1177/0959683615580201

Large, D. J., Spiro, B., Ferrat, M., Shopland, M., Kylander, M., Gallagher, K., et al. (2009). The influence of climate, hydrology and permafrost on Holocene peat accumulation at 3500m on the eastern Qinghai–Tibetan Plateau. *Quaternary Science Reviews*, *28*(27–28), 3303–3314. https://doi.org/10.1016/j.quascirev.2009.09.006

Larsson, A., Segerström, U., Laudon, H., & Nilsson, M. B. (2017). Holocene carbon and nitrogen accumulation rates in a boreal oligotrophic fen. *The Holocene*, *27*(6), 811–821. https://doi.org/10.1177/0959683616675936

Leng, X. T., Wang, S. Z., Zhao, H. Y., Lin, Q. H., & Hong, B. (2003). Composition, physiochemical properties and water-chemistry environment analysis on the oligotrophic peat. *Bulletin of Mineralogy, Petrology and Geochemistry*, *22*, 114–119. (In Chinese)

Limpens, J., Heijmans, M. M. P. D., & Berendse, F. (2006). The nitrogen cycle in boreal peatlands. In R. Wiederm, & D. Vitt (Eds.), *Boreal peatland ecosystems (ecological studies)* (pp. 195–230). Berlin; Heidelberg: Springer-Verlag.

Loisel, J., & Garneau, M. (2010). Late-Holocene paleoecohydrology and carbon accumulation estimates from two boreal peat bogs in eastern Canada: Potential and limits of multi-proxy archives. *Palaeogeography, Palaeoclimatology, Palaeoecology*, *29*, 493–533.

Loisel, J., Yu, Z., Beilman, D. W., Camill, P., Alm, J., Amesbury, M. J., & Belyea, L. R. (2014). A database and synthesis of northern peatland soil properties and Holocene carbon and nitrogen accumulation. *The Holocene*, *24*(9), 1028–1042. https://doi.org/10.1177/0959683614538073

Luo, C. X., Zheng, Z., Tarasov, P., Pan, A. D., Huang, K. Y., Beaudouin, C., & An, F. Z. (2009). Characteristics of the modern pollen distribution and their relationship to vegetation in the Xinjiang region, northwestern China. *Review of Palaeobotany and Palynology*, *153*(3–4), 282–295. https://doi.org/10.1016/j.revpalbo.2008.08.007

Madsen, D. B., Chen, F., Oviatt, C. G., Zhu, Y., Brantingham, P. J., Elston, R. G., & Bettinger, R. L. (2003). Late Pleistocene/Holocene wetland events recorded in southeast Tengger Desert lake sediments, NW China. *Chinese Science Bulletin*, *48*(14), 1423–1429. https://doi.org/10.1360/02wd0257

Malmer, N., Svensson, B. M., & Wallén, B. (1994). Interactions between *Sphagnum* mosses and field layer vascular plants in the development of peat-forming systems. *Folia Geobotanica et Phytotaxonomica*, *29*(4), 483–496. https://doi.org/10.1007/BF02883146

McLauchlan, K. K., Williams, J. J., Craine, J. M., & Jeffers, E. S. (2013). Changes in global nitrogen cycling during the Holocene epoch. *Nature*, *495*(7441), 352–355. https://doi.org/10.1038/nature11916

Moore, T. R., Bubier, J. L., & Frolking, S. (2002). Plant biomass and production and CO_2 exchange in an ombrotrophic bog. *Journal of Ecology*, *1*, 25–36.

Olid, C., Nilsson, M. B., Eriksson, T., & Klaminder, J. (2014). The effects of temperature and nitrogen and sulfur additions on carbon accumulation in a nutrient-poor boreal mire: Decadal effects assessed using ^{210}Pb peat chronologies. *Journal of Geophysical Research: Biogeosciences*, *119*, 392–403. https://doi.org/10.1002/2013JG002365

Page, S. E., Rieley, J. O., & Wüst, R. (2006). Lowland tropical peatlands of Southeast Asia. *Developments in Earth Surface Processes*, *9*, 145–172. https://doi.org/10.1016/S0928-2025(06)09007-9

Panait, A., Diaconu, A., Galka, M., Grindean, R., Hutchinson, S. M., Hickler, T., et al. (2017). Hydrological conditions and carbon accumulation rates reconstructed from a mountain raised bog in the Carpathians: A multi-proxy approach. *Catena*, *152*, 57–68. https://doi.org/10.1016/j.catena.2016.12.023

Smith, L., MacDonald, G., Velichko, A., Beilman, D., Borisova, O., Frey, K., et al. (2004). Siberian peatlands: A net carbon sink and global methane source since the early Holocene. *Science*, *303*(5656), 353–356. https://doi.org/10.1126/science.1090553

Sun, J. H. (2012). Holocene environment changes inferred from the plant macrofossil records from the peatlands in Altai Mountains, Xinjiang (Master Thesis). Lanzhou University, Lan Zhou, China, 19.

Tarnocai, C., Canadell, J. G., Schuur, E. A., Kuhry, P., Mazhitova, G., & Zimov, S. (2009). Soil organic carbon pools in the northern circumpolar permafrost region. *Global Biogeochemical Cycles*, *23*, GB2023. https://doi.org/10.1029/2008GB003327

Turunen, J., Tomppo, E., Tolonen, K., & Reinikainen, A. (2002). Estimating carbon accumulation rates of undrained mires in Finland-application to boreal and subarctic regions. *The Holocene*, *12*(1), 69–80. https://doi.org/10.1191/0959683602hl522rp

Wallén, B., & Malmer, N. (1992). Distribution of biomass along hummock-hollow gradients: A comparison between a North American and Scandinavian peat bog. *Acta Societatis Botanicorum Poloniae*, *61*, 75–87.

Wang, W., & Zhang, D. (2019). Holocene vegetation evolution and climatic dynamics inferred from an ombrotrophic peat sequence in the southern Altai Mountains within China. *Global and Planetary Change*, *179*, 10–22. https://doi.org/10.1016/j.gloplacha.2019.05.003

Wang, Y. J., Cheng, H., Edward, R. L., He, Y. Q., Kong, X. G., An, A. S., & Wu, J. Y. (2005). The Holocene Asian monsoon: Link to solar changes and North Atlantic climate. *Science*, *308*(5723), 854–857. https://doi.org/10.1126/science.1106296

Xing, W., Bao, K. S., Guo, W. Y., Lu, X. G., & Wang, G. P. (2015). Peatland initiation and carbon dynamics in northeast China: Links to Holocene climate variability. *Boreas*, *3*, 575–587.

Yang, Y. P., Zhang, D. L., Lan, B., Abdusalih, N., & Feng, Z. D. (2019). Peat δ^{13}C celluose-signified moisture variations over the past ~2200 years in the southern Altai Mountains, northwestern China. *Journal of Asian Earth Sciences*, *174*, 59–67. https://doi.org/10.1016/j.jseaes.2018.11.019

Yu, Z. (2012). Northern peatland carbon stocks and dynamics: A review. *Biogeosciences*, *9*(10), 4071–4085. https://doi.org/10.5194/bg-9-4071-2012

Yu, Z., Beilman, D. W., & Jones, M. C. (2009). Sensitivity of northern peatland carbon dynamics to Holocene climate change. In A. Baird, L. Belyea, X. Comas, et al. (Eds.), *Northern peatlands and carbon cycling (American Geophysical Union Monograph Series)* (pp. 55–69). Washington, DC: American Geophysical Union.

Yu, Z., Loisel, J., Brosseau, D. P., Beilman, D. W., & Hunt, S. J. (2010). Global peatland dynamics since the Last Glacial Maximum. *Geophysical Research Letters*, *37*, L13402. https://doi.org/10.1029/2010GL043584

Zhang, D. L., & Feng, Z. D. (2018). Holocene climate variations in the Altai Mountains and the surrounding areas: A synthesis of pollen records. *Earth-Science Reviews*, *185*, 847–869. https://doi.org/10.1016/j.earscirev.2018.08.007

Zhang, Y., Meyers, P. A., Liu, X. T., Wang, G. P., Ma, X. H., Li, X. Y., et al. (2016). Holocene climate changes in the central Asia mountain region inferred from a peat sequence from Altai Mountains, Xinjiang, northwestern China. *Quaternary Science Reviews*, *152*, 19–30. https://doi.org/10.1016/j.quascirev.2016.09.016

Zhang, Y., Yang, P., Tong, C., Liu, X., Zhang, Z., Wang, G., & Meyers, P. A. (2018). Palynological record of Holocene vegetation and climate changes in a high-resolution peat profile from the Xinjiang Altai Mountains, northwestern China. *Quaternary Science Reviews*, *201*, 111–123. https://doi.org/10.1016/j.quascirev.2018.10.021

Zhao, Y., Yu, Z., Tang, Y., Li, H., Yang, B., Li, F. R., et al. (2014). Peatland initiation and carbon accumulation in China over the last 50,000 years. *Earth-Science Reviews*, *128*, 139–146. https://doi.org/10.1016/j.earscirev.2013.11.003

Zhao, Y., Yu, Z. C., Zhang, J. W., & Yang, B. (2009). Vegetation response to Holocene climate change in monsoon-influenced region of China. *Earth-Science Reviews*, *97*(1–4), 242–256. https://doi.org/10.1016/j.earscirev.2009.10.007